Ignjatović, N.L., K.M. Penov-Gaši, J.J. Ajduković, V.V. Kojić, S.B. Marković, and D.P. Uskoković. 2018. "The Effect of the Androstane Lung Cancer Inhibitor Content on the Cell-Selective Toxicity of Hydroxyapatite-Chitosan-PLGA Nanocomposites." *Materials Science and Engineering C* 89: 371–77. https://doi.org/10.1016/j.msec.2018.04.028.

The effect of the androstane lung cancer inhibitor content on the cell-selective toxicity of hydroxyapatite-chitosan-PLGA nanocomposites

Nenad L. Ignjatović[1*], Katarina M. Penov-Gaši[2], Jovana J. Ajduković[2], Vesna V. Kojić[3], Smilja B. Marković[1], Dragan P. Uskoković[1]

[1]Institute of Technical Sciences of the Serbian Academy of Science and Arts, Knez Mihailova 35/IV, P.O. Box 377, 11000 Belgrade, Serbia

[2]University of Novi Sad, Faculty of Sciences, Department of Chemistry, Biochemistry and Environmental Protection, Trg Dositeja Obradovića 3, 21000 Novi Sad, Serbia

[3]University of Novi Sad, Faculty of Medicine, Oncology Institute of Vojvodina, Put Dr Goldmana 4, 21204 Sremska Kamenica, Serbia

[*]Corresponding author: nenad.ignjatovic@itn.sanu.ac.rs

Abstract

An androstane (17β-hydroxy-17α-picolyl-androst-5-en-3β-yl-acetate (derivative A)) cancer inhibitor was successfully captured in a carrier made of nano-sized hydroxyapatite (HAp) coated with chitosan-PLGA polymer blends (Ch-PLGA). In our previous studies, we demonstrated that it was convenient to use spherical HAp/Ch-PLGA carriers as vehicles to target the lungs following intravenous administration. In this study, we used emulsification and subsequent freeze-drying to load the spherical HAp/Ch-PLGA carriers with varying contents of the derivative A, in order to examine the selective toxicity towards cancerous/healthy lung cells. The XRD and FT-IR techniques confirmed the drug loading process, and the content of the poorly water soluble derivative A was estimated directly via the DSC technique. The particles were spherical in shape with the d_{50} distribution varying

between 167 and 231 nm, whereas the content of the derivative A ranged from 6.5 to 19.3 wt%. Cell-selective cytotoxicity was examined simultaneously on two cell lines: human lung carcinoma (A549 ATCC CCL 185) and human lung fibroblasts (MRC-5 ATCC CCL 171). All particles exhibited nearly three times larger cytotoxicity towards cancer cells (A549) than towards healthy cells (MRC5), where the particles with the derivative A content of 6.5wt% allowed for the viability of healthy cells greater than 80%. Ninety-six hours after the treatment of cells with particles with different contents of derivative A (after incubation and recovery), recovery was faster in damaged healthy cells than in cancerous cells.

Key words: androstane; hydroxyapatite; nano-carrier; lung cancer; cell-selective cytotoxicity.

Introduction

Calcium phosphates, especially hydroxyapatite (HAp), as the most common inorganic bone component [1], have a high potential for use in preventive and regenerative medicine [2, 3]. The past decade has witnesses a significant growth of research into the application of HAp particles, not only as a material for the reconstruction of bone tissue but also as a drug carrier in biomedicine [4]. Hydroxyapatite nanoparticles (HApNs) have shown selective anti-cancer activity in the treatment of lung cancer. The cytotoxic activity of HApNs towards human lung cancer cells (A549) has been demonstrated to be significant, without affecting the survival of normal bronchial epithelial 16HBE cells [5]. The research aimed at creating new functional and hybrid systems based on HAp largely expands the potential for its application for biomedical purposes [6]. In our previous study, we examined the possibility of applying multifunctional and hybrid systems based on HAp and bioresorbable polymers in the reconstruction of bone tissue damaged by osteoporosis [7, 8].

Nano-carriers for cancer inhibitors are a promising strategy in increasing the treatment efficiency for various types of cancer, accompanied with an increased toxicity towards cancer cells and decreased toxicity towards healthy cells [9]. Lung cancer is one of the most common and the most lethal cancer types at a global level [10]. An analysis of the delivery efficiency of nanoparticles in different tumor types indicates that it is the lowest in cases of lung tumors. [11]. There are different strategies seeking not only to improve the delivery efficiency, but also to increase the drug content in the carrier. One of them is to design a synthetic system where the system/carrier molecules would firmly grip and entrap the drug. These cage nanoparticles could be promising vehicles for continuous drug delivery [12].

Biodegradable polymer particles based on poly-lactide-co-glycolide (PLGA) have been used as suitable vehicles for various cancer inhibitors targeting the lungs after intravenous application [13]. Core-shell particles based on PLGA and linear polysaccharide chitosan (Ch) loaded with cancer inhibitors have shown a high potential in the treatment of lung cancer [14, 15]. PLGA nanoparticles modified with Ch have also shown a high potential as nano-carriers of poorly hydrophilic drugs in the treatment of breast cancer [16]. Dual-drug containing core–shell nanoparticles based on PLGA and Ch were designed to reduce and eliminate toxicity to healthy human cells in potential lung cancer therapy and their efficiency was tested. Particles with the hydrodynamic diameter of 289±49 nm were cyto- and chemo-compatible, and they operated by targeting folate receptors [17]. During *in vivo* studies, it was found that after the intravenous application of spherical nano-HAp-based particles coated with a polymeric PLGA-Ch blend, they were accumulated in the lungs [18, 19]. Spherical HAp/Ch-PLGA particles with hydrodynamic properties that allow to direct them towards the lungs following injection could play the role of vehicles in drug delivery for various lung diseases. Polymer components that coat nano-HAp particles could be optimal for the entrapment of various drugs. A wide variety of different androstane derivatives with a

heterocyclic ring showed a high potential as cancer inhibitors in the treatment of hormone-dependent cancers [20–22].

In our previous research, we examined the possibility of synthesizing and designing HAp/Ch-PLGA spherical particles loaded with17β-hydroxy-17α-picolyl-androst-5-en-3β-yl-acetate (A). The results of *in vitro* tests indicated selective A-HAp/Ch-PLGA activity; the particles did not exhibit cytotoxicity towards primary mouse lung fibroblasts (C57BL/6) but they were cytotoxic for lung cancer cells [23]. In the present study, we demonstrate the synthesis and design of spherical HAp/Ch-PLGA particles loaded with varying contents of an androstane-based cancer inhibitor (17β-hydroxy-17α-picolyl-androst-5-en-3β-yl-acetate, A). The influence of the content of androstane derivative on the morphology and size distribution of the synthesized particles was also examined. The content of androstane derivatives in all systems was determined directly using the DSC technique. The electrokinetic parameters of all particles as potential activity indicator in the middle particle layer – biological environment were determined by measuring zeta potential, electrophoretic mobility and conductivity. The influence of the content of the androstane-based cancer inhibitor A on cell-selective toxicity was examined simultaneously on two cell lines: on human lung carcinoma (A549) and human lung fibroblasts (MRC-5) using dye exclusion (DET) and MTT assays. The viability of both cell types after the treatment with synthesized particles was also examined in order to quantify the selective activity.

2. Experimental

2.1. Synthesis of materials

2.1.1. Synthesis of 17β-hydroxy-17*α*-picolyl-androst-5-en-3β-yl acetate (A)

The first stage in the preparation of 17β-hydroxy-17α-picolyl-androst-5-en-3β-yl-acetate (A) was the addition of α-picolyllithium to the 17-oxo group of dehydroepiandrosterone, resulting in 17α-picolyl-androst-5-en-3β,17β-diol. This was followed by acetylation using acetic anhydride in absolute pyridine at room temperature for 3 h [24, 25].

2.1.2. Synthesis of HAp, HAp/Ch-PLGA and A-loaded HAp/Ch-PLGA

An aqueous calcium nitrate ($Ca(NO_3)_2$) solution (150 ml; 26.6 wt.%) was added to the solution of ammonium phosphate ($(NH_4)_3PO_4$) (7 ml H_3PO_4+165 ml NH_4OH+228 ml H_2O) at 50°C over the period of 60 minutes, while stirring at the rate of 100 rpm. The solution was then subjected to a heat treatment at 100°C for 60 minutes. The resulting gel was dried at room temperature in a vacuum drier for 72 h, after which the final product – HAp powder - was obtained. X-ray diffraction run on the HAp powder confirmed its poorly crystalline nature, whereas the PSD technique enabled us to determine the particle size of d_{50}=70 nm [26].

Chitosan (Ch) of a low molecular weight (Aldrich, deacetylation>75%), dissolved in acetic acid (1 wt.%), was mixed with 17β-hydroxy-17*α*-picolyl-androst-5-en-3β-yl acetate powder (A) in the weight ratio according to Table 1, while stirring with a magnetic stirrer at 400 rpm. PLGA (50:50, Sigma, USA) dissolved in acetone was mixed with the A-containing Ch solution and HAp gel in the 2:3:5 weight ratio. A water solution of poloxamer 188 (polyethylenepolypropylene glycol, 0.1 vol.%) was added drop-wise to the resulting mixture, while stirring at 21,000 rpm. The obtained mixture of A, chitosan, PLGA and HAp was slowly poured into a glutaraldehyde solution (Grade I, 25% in H_2O), while stirring at 21,000 rpm for 1 h. The obtained mixture was then centrifuged at 3000 rpm and 5°C for 1 h, and the resulting precipitate was subjected to lyophilization at temperatures ranging from -10 to -60°C and pressures ranging from 0.37 mbar to 0.1 mbar for 1 to 8h [23]. The obtained powder was

washed with distilled water three times, centrifuged at 1000 rpm and dried again. The final product was the powder composed of HAp particles coated with A-loaded chitosan-poly(D,L)-lactide-co-glycolide (Tab. 1).

Table 1. The projected content of A in A-loaded HAp/Ch-PLGA

2.2. Characterization of the products

X-Ray diffraction (XRD) was performed on a Philips PW-1050 diffractometer with Ni-filtered $Cu_{K\square}$ radiation, the scanning step was 0.02°. The particle size distribution (PSD) was measured on 10 mg/ml of powders dispersed in water using a Mastersizer 2000 (Malvern Instruments Ltd.) and a *HydroS* dispersion unit for liquid dispersants. Morphological characterization was performed using an atomic force microscope (AFM, Thermo Microscopes, Autoprobe CP Research). Content of HAp in the particles was determined by simultaneous TG–DTA (Setsys 2400 CS Evolution, SETARAM Instrumentation, Caluire, France) in the temperature range between 30 and 600 °C with the heating rate of 10 °min^{-1} and under the air flow of 20 ml·min^{-1}. Differential scanning calorimetry (DSC) measurements were performed on an Evo 131 (Setaram Instrumentation) differential scanning calorimeter. Samples were analyzed in nitrogen by heating (10°/min) from 25 to 360°C. Infrared spectroscopy (FT-IR) was done on a Nicolet iS10 FT-IR Spectrometer (Thermo Scientific Instruments) in the spectral range from 400 to 4000 cm^{-1}. Electrokinetic parameters of the suspensions of synthesized particles were analyzed using a Zeta-Sizer Nano (Malvern Instruments Ltd.) in deionized water and pH 7.0.

2.3 *In vitro* tests

2.3.1 Cell lines

Toxicity tests were carried out on two cell lines, human lung carcinoma (A549 ATCC CCL 185) and human lung fibroblasts (MRC-5 ATCC CCL 171) which grew adhered to the dish floor (Costar, 25cm^3) in Dulbecco's modified Eagle's medium (DMEM, Gibco BRL, UK) with 4.5 g/l glucose and 10% FCS (fetal calf serum, Sigma). The medium contained antibiotics: penicillin 100 IU/ml and streptomycin 100 μg/ml. The cell lines were maintained under standard conditions: at the temperature of 37°C in a humidity saturated atmosphere with 5% CO2 (Heraeus). The cells were passaged twice a week, and in the experiments the cells were used in the logarithmic growth phase between the third and tenth passages. Only viable cells were used. The number of cells and their viability were determined by a color rejection test with 0.1% trypan blue.

2.3.2 DET - Dye exclusion test

The cells were centrifuged (10 min/200xg) and counted in 0.1% trypan blue. Viable cells were sown in Petri cups (Center well, Falcon) containing the examined substance/disc at a concentration of 2×10^5/ml. Control samples did not contain the test substance. Petri cups with seeded cells were left at 37°C, with 5% CO_2 for 48 hours (h). After incubation, cell counting was performed using an inverted microscope (REICHERT) in counting chambers. Cytotoxicity was expressed as a percentage according to the formula: $CI = (1-N_s/N_k) \cdot 100$, where N_k is the number cells in the control samples, and N_s is the number of cells in the samples with the tested substance.

2.3.3. Colorimetric test with tetrazolium salts (MTT test)

The cells were harvested in the logarithmic growth stage, sedimented by centrifugation (10 min/200 xg) and counted in 0.1% trypan blue. The viable cells were sown in Petri cups (Center well, Falcon) containing the tested substances/discs at a concentration of 2×10^5/ml.

The control samples did not contain the test substances. Petri cups with seeded cells were left in a thermostat at 37ºC, with 5% CO_2 for 48 hours. Viable cells were seeded ($5x10^3$ /100µl) in quadruplicate in 96-well microtiter plates. The plates with seeded cells were left in a thermostat at 37ºC, with 5% CO2 for 48 h. MTT solution, prepared immediately prior to addition, was added to all plate wells in the 10 µl/well volume and incubation was continued for 3h (in a 37°C thermostat with 5% CO_2). After 3h, 100 µl of 0.04 mol /l HCl in isopropanol was added to each well. The absorbance was read immediately after the incubation period on the microtiter plate reader (Multiscan, MCC/340) at a wavelength of 540 nm and a reference of 690 nm. The wells on the plate that contained only the medium and MTT, but not the cells, served as blank [27]. Cytotoxicity was expressed as a percentage according to the formula: CI = (1-As/Ak)x100, whereby Ak is the absorbance of the control samples, and As is the absorbance of the samples with the test substance.

3. Results and discussion

Figure 1 shows the diffractograms of A, HAp/Ch-PLGA and A-loaded HAp/Ch-PLGA. The androstane derivative (A) is characterized by peaks at the positions 14.7°, 15.6°, 17.4° and 18.8°. The most intense peaks were recorded at 31.8° (2 1 1), 32.2° (1 1 2), 32.9° (3 0 0), 25.9° (0 0 2) and 49.5° (2 1 3) and they originated from poorly crystalline, non-stoichiometric HAp [18]. The HAp/Ch-PLGA diffractogram confirms the presence of HAp and Ch. Namely, in addition to characteristic HAp peaks, two reflections detected at 10.2° and 19.8° originated from Ch [28]. The absence of PLGA peaks on the diffractograms indicates that the polymer is amorphous, as confirmed in our earlier XRD studies. The presence of characteristic peaks of derivative A in diffractograms of $A_{1,\ 2\ and\ 3}$-HAp/Ch-PLGA powders qualitatively confirms the presence of A in A-HAp/Ch-PLGA.

Figure 1. XRD of A, HAp/Ch-PLGA, A_1-HAp/Ch-PLGA, A_2-HAp/Ch-PLGA and A_3-HAp/Ch-PLGA

The morphology and distribution of particle size of the synthesized powders $A_{1,2 \text{ and } 3}$-HAp/Ch-PLGA is shown in Figure 2. A_1-HAp/Ch-PLGA particles have d_{10} = 135 nm; d_{50}=67 nm and d_{90}= 42 nm. The A_2-HAp/Ch-PLGA system has the distribution values d_{10} =135 nm, d_{50}=168 nm and d_{90}=247 nm, and A_3-HAp/Ch-PLGA d_{10}=162 nm, d_{50}=231 nm and d_{90}=453 nm (Figure 2a-c). A general trend of increased average particle sizes (d_{50}) with an increased content of the derivative A was observed. The surface morphology of $A_{1, 2 \text{ and } 3}$-HAp/Ch-PLGA was analyzed using AFM in a non-contact mode. All three types of particles had similar spherical morphologies.

Figure 2. PSD and AFM of particles: a) A_1-HAp/Ch-PLG, b) A_2-HAp/Ch-PLGA and c) A_3-HAp/Ch-PLGA

Figure 3 shows the IR spectra of A, A_1-HAp/Ch-PLGA, A_2-HAp/Ch-PLGA and A_3-HAp/Ch-PLGA. The wide IR band in the spectrum of A (17β-hydroxy-17α-picolyl-androst-5-ene-3β-yl acetate) with a maximum of about 3300 cm^{-1} was assigned to the stretching vibration of the OH group (17β-OH). Several absorption bands at about 2943 and 2827 cm^{-1} came from the alkyl stretching vibrations of the -CH group (from $-CH_3$ and $=CH_2$). The valent vibrations of the acetate group were recorded as sharp bands with a maximum of about 1242 cm^{-1}, which is in line with the studies of other authors [29, 23]. The presence of the characteristic bands of pure derivative A was also established in the particle spectra of all three systems, which qualitatively confirms the presence of derivative A in the particles

HAp/Ch-PLGA. In all spectra of the A_1-HAp/Ch-PLGA, A_2-HAp/Ch-PLGA and A_3-HAp/Ch-PLGA particles, the characteristic bands of HAp, Ch and PLGA were also observed. The characteristic bands at about 1030 cm^{-1} and 1080 cm^{-1} could be assigned to the vibration of the PO_4^{3-} group of HAp and the band at 3552 cm^{-1} to vibration of the OH- group. The absorption band at about 563 cm^{-1} was assigned to the bending mode of the PO_4^{3-} group [30]. Other significant bands originated from PLGA and Ch: -C=O stretching vibrations at about 1725 cm^{-1}, weak sharp bands at around 1655 cm^{-1} and 1580 cm^{-1} were assigned to Amid I and II vibrations, etc. [31-33]. In accordance with the methodology of introducing derivative A into the initially dissolved polymer PLGA and Ch (section 2.1.2.), in addition to the XRD results (Figure 1), IR results also qualitatively confirmed the encapsulation of derivative A by the used polymers.

Figure 3. ATR FTIR spectra of A, A_1-HAp/Ch-PLGA, A_2-HAp/Ch-PLGA and A_3-HAp/Ch-PLGA

The amount of HAp in the particles was determined by a TG-DTA analysis. The results of the TG-DTA analyses of derivate A, Ch, PLGA, A_1-HAp/Ch-PLGA, A_2-HAp/Ch-PLGA and A_3-HAp/Ch-PLGA in the 30-600 °C temperature range are shown in Fig. 4. The TGA curves of A (Fig, 4a), Ch (Fig. 4b) and PLGA (Fig. 4c) show complete degradation at 600 °C (100% mass loss). These results suggest that the residue in the composites (Fig. 4.d,e,f) originate from HAp. The TGA curve for A_1-HAp/Ch-PLGA shown in Fig. 4a reveals a 52±0.5 % weight loss at 600°C. The residue of 48±0.5% in weight is only due to HAp. Similar results were obtained for composites A_2-HAp/Ch-PLGA and A_3-HAp/Ch-PLGA (Fig. 4e,f). The TGA curves for A_2-HAp/Ch-PLGA and A_3-HAp/Ch-PLGA show a 53±0.5% % weight loss at 600°C. The obtained results indicate that the residue of 47±0.5% % wt. contains HAp. As can

be seen from Fig 4d,e,f, the DTA curves of A-loaded HAp/Ch-PLGA are dominated by peaks characteristic for the pure compounds A, Ch and PLGA. The sequence of broad exothermic peaks originating from the degradation of Ch and PLGA is observed in each of the examined systems. The degradation mechanism of Ch and PLGA involve a random chain scission at the beginning of decomposition and a specific chain scission at the end. The TGA curves for A_1-HAp/Ch-PLGA, A_2-HAp/Ch-PLGA and A_3-HAp/Ch-PLGA show no mass loss when exposed to the temperature range in which the evaporation and degradation of A, Ch and PLGA occur. This observation is in agreement with the DTA curves.

Figure 4. TGA/DTA of a) A_1, b) Ch, c) PLGA, d) A_1-HAp/Ch-PLGA, e) A_2-HAp/Ch-PLGA and f) A_3-HAp/Ch-PLGA

Differential scanning calorimetry (DSC) has proved to be suitable for determining the content of poorly water-soluble drugs in various pharmaceutical products, based on the measurement of phase transition enthalpy [34]. Androstane derivative A belongs to the group of poorly water-soluble compounds and its DSC thermogram is shown in Figure 5. The endothermic phase transition dominates the DSC thermogram of derivative A with a sharp endothermic peak centered at 213.8^{o}C (onset 211.4^{o}C, offset 215.4^{o}C). The same phase transition is also noticeable on the thermograms of the A_1-HAp/Ch-PLGA, A_2-HAp/Ch-PLGA and A_3-HAp/Ch-PLGA particles (Figure 5). The wide endothermic doublet (onset 49.4°C, offset 131.5°C) originates from the PLGA and Ch transformation [35, 36]. The exothermic peak at higher temperatures (onset 293.1°C, offset 329.4°C) comes from the deacetylation of Ch. By integrating the endothermic peaks of the characteristic phase transition of pure (100%) and encapsulated derivative A, the obtained enthalpy values (ΔH) are shown in Table 2. Based on a comparison of the enthalpy values of pure and encapsulated derivative A, it can be argued that the content of the encapsulated derivative A in A_1-

HAp/Ch-PLGA 6.5%, in A_2-HAp/Ch-PLGA 9.2% and in A_3-HAp/Ch-PLGA 19.3%. The presented results are the average values obtained on three identically prepared samples.

Figure 5. DSC of A, A_1-HAp/Ch-PLGA, A_2-HAp/Ch-PLGA and A_3-HAp/Ch-PLGA

Tabele 2. Enthalpy and content of A according to the DSC results

Electrokinetic parameters are important not only for particle–particle interactions, but also for interactions between particles and the biological environment [36]. The influence of the zeta potential (-10.28 to -29.65 mV) of HAp particles on cellular uptake in human monocyte-macrophage cells was examined. It was found that particles with less negative values of zeta potential achieved a greater uptake [38, 39]. The results of zeta potential measurements for the particles based on poorly crystalline HAp showed that the presence of polysaccharides on the particle surface greatly increased their efficacy as nanocarriers in controlled drug delivery [40]. Table 3 shows the values of the zeta potential, electrophoretic mobility and conductivity of A_1-HAp/Ch-PLGA, A_2-HAp/Ch-PLGA and A_3-HAp/Ch-PLGA particles. In general, the particles that have zeta potential values between 0 and ±15mV are prone to flocculation and aggregation, while absolute ZP values greater than 15mV are typical of stable and aggregately resistant particles [41, 42]. The most prone to aggregation were A_1-HAp/Ch-PLGA particles, less so A_2-HAp/Ch-PLGA, while A_3-HAp/Ch-PLGA particles were the most stable. The ZP values also served as a tool in the study of comparative interactions of nanoparticles with healthy and breast cancer cells. A difference in surface charge was observed between healthy and cancerous breast cells (MCF10A and MCF7), as well as different interaction types and intensities between the same nanoparticles and healthy/cancerous cells [43]. Based on the results shown in Table 3, it was expected that all

three types of the synthesized particles would exhibit a different activity towards healthy/cancerous cells, which was also investigated in subsequent *in vitro* studies.

In addition to a small difference in the particle sizes d_{50} of all three systems (Figure 2), the basic difference is reflected in the fraction of the derivative A (Table 2). With an increased content of derivative A in the particles, a change was expected in the content of the surface groups and ions resulting from the dissociation of the derivatives. Changes in the ionic composition of the nanoparticle environment can result in the appearance of specific and non-specific ion effects [44]. The reduction of the mobility value and an increased conductivity that accompanied the increased content of derivative A in the system were most likely the result of ion effects rather than the difference in particle sizes.

Table 3. Zeta potential, electrophoretic mobility and conductivity of A_1-HAp/Ch-PLGA, A_2-HAp/Ch-PLGA and A_3-HAp/Ch-PLGA particles (ξ—zeta potential; u_e—mobility; K-conductivity).

Figure 6 shows the results of the testing of the cytotoxicity and viability of healthy and cancerous lung cells (MRC5 and A549) after incubation with A, drug free HAp/Ch-PLGA, A_1-HAp/Ch-PLGA, A_2-HAp/Ch-PLGA and A_3-HAp/Ch-PLGA performed using DET and MTT assays. The results of the comparative cytotoxicity tests of A_1-HAp/Ch-PLGA, A_2-HAp/Ch-PLGA and A_3-HAp/Ch-PLGA particles towards MRC5 and A549 cells are shown in Figure 6a. As the content of A increased in the HAp/Ch-PLGA carrier, the particles exhibited more intensive cytotoxicity towards both cell lines. Cytotoxic activity is significantly more pronounced towards lung cancer cells (A549) than to healthy cells (MRC5), almost three times for each type of particles with derivative A. The cell viability results were obtained after 48 h of incubation with the particles of A_1-HAp/Ch-PLGA, A_2-HAp/Ch-PLGA and A_3-

HAp/Ch-PLGA, washing and counting in 0.1% trypan blue (Fig. 6b). With an increased content of derivative A in the carrier, the achieved cellular viability decreased. Based on the results shown in Figure 6b, it is clear that the viability of healthy cells (MRC5) is always higher than that of malignant cells (A549) in all three investigated systems with different contents of derivative A. The viability of healthy cells (MRC5) was higher than 80% for the particles of A_1-HAp/Ch-PLGA (82.12%), while for A_2-HAp/Ch-PLGA and A_3-HAp/Ch-PLGA it was lower than 80% (69.67 and 62.12%). After an 48-hour incubation with particles of A_1-HAp/Ch-PLGA, A_2-HAp/Ch-PLGA and A_3-HAp/Ch-PLGA, both cell lines (MRC5 and A549) were left to recover for 48 h and the obtained cytotoxicity results are shown in Figure 6c. After the recovery, the cytotoxicity values were more pronounced in malignant cells (A549) than in healthy ones (MRC5), which demonstrates a more intensive recovery of healthy cells, compared to the malignant ones. The action mechanism of synthetic androstane derivatives on hormone-dependent cancer cells has not been fully elucidated. Previous *in vitro* and *in vivo* tests with androstane derivatives indicated their unique properties, such as tissue-selective cytotoxicity, target specificity and implications for the treatment of inoperable malignancies [45].

Figure 6. *In vitro* test of A_1-HAp/Ch-PLGA, A_2-HAp/Ch-PLGA and A_3-HAp/Ch-PLGA on two cell lines: regular MRC5 human lung fibroblasts and A549 human lung carcinoma cells: a) cytotoxicity and b) viability estimated using dye exclusion test (DET); c) cytotoxicity following a 48-hour recovery period estimated using the MTT (3-(4,5-Dimethylthiazol-2-yl)-2,5-diphenyltetrazolium bromide) assay.

The path of energy modulation of cancer cells (A549) is different from that of healthy cells (MRC5). In previous research, it was established that, in contrast to normal cells, cancer

cells may lose the ability to utilize aerobic respiration due to either defective mitochondria or hypoxia within tumor microenvironments [46]. The cytotoxicity results show that MRC5 cells are less sensitive than A549 cells, which are more susceptible to the action of A-loaded HAp/Ch-PLGA. This leads to a reduced recovery capacity.

4. Conclusion

Spherical particles were created as suitable vehicles for varying contents of a poorly water soluble androstane derivative, 17β-hydroxy-17α-picolyl-androst-5-en-3β-yl-acetate (A), from nano-sized hydroxyapatite (HAp) coated with a polymer blend consisting of chitosan (Ch) poly-lactide-co-glycolide (PLGA). XRD and FT-IR analyses confirmed the efficiency of the drug loading process and the DSC technique determined the content of derivative A in the HAp/Ch-PLGA carriers, which was 6.5wt%, 9.2wt%, and 19.3wt%. As the content of derivative A increased, so did the median value of the particle size distribution – particles with 6.5wt% A had d_{50} 167 nm, with 9.2wt% 168 nm and with 19.3wt% 231 nm. An increased content of derivative A in the carrier reduced the values of zeta potential and electrophoretic mobility and increased the conductivity of the particles, most likely due to changes in the ionic environment around the particles. The anti-cancer selectivity of the particles was confirmed on two cell lines: human lung carcinoma (A549) and human lung fibroblasts (MRC-5) using dye exclusion (DET) and MTT assays. All types of A-loaded HAp/Ch-PLGA showed almost three times larger cytotoxicity towards cancerous cells than to healthy ones. Forty-eight hours after the treatment of both types of cells with the particles of HAp/Ch-PLGA loaded with A (6.5wt.%) that had the lowest zeta potential (-9.61±0.37 mV), the viability of healthy cells was 82.12%. The particles with the lowest zeta potential (-33.3±2.35 mV) for HAp/Ch-PLGA loaded with A (19.3 wt%) were the most cytotoxic to both

cell lines (A549 and MRC-5). Ninety-six hours after the treatment of both types of cells with the particles of A-loaded HAp/Ch-PLGA, for all contents of derivative A, the recovery of damaged healthy cells was observed to be two and three times faster than that of cancerous cells.

Acknowledgments

The research presented in this paper was supported by the Ministry of Education, Science and Technological Development of the Republic of Serbia (project No. III45004). The authors acknowledge the help of Dr. Kata Trifković of the Faculty of Technology and Metallurgy, University of Belgrade, for the zeta potential measurements. The authors would also like to thank to Dr. Ljilijana Veselinović for XRD measurements and Dr. Dana Vasiljević-Radović for the AFM analysis.

References

[1] J.F. Osborn, H. Newesely, The material science of calcium phosphate ceramics, Biomaterials. 1 (1980) 108–111. doi:10.1016/0142-9612(80)90009-5.

[2] W. Habraken, P. Habibovic, M. Epple, M. Bohner, Calcium phosphates in biomedical applications: Materials for the future?, Mater. Today. 19 (2016) 69–87. doi:10.1016/j.mattod.2015.10.008.

[3] S. Bose, S. Tarafder, Calcium phosphate ceramic systems in growth factor and drug delivery for bone tissue engineering: A review, Acta Biomater. 8 (2012) 1401–1421. doi:10.1016/j.actbio.2011.11.017.

[4] A. Haider, S. Haider, S.S. Han, I.-K. Kang, Recent advances in the synthesis,

functionalization and biomedical applications of hydroxyapatite: a review, RSC Adv. 7 (2017) 7442–7458. doi:10.1039/C6RA26124H.

[5] Y. Sun, Y. Chen, X. Ma, Y. Yuan, C. Liu, J. Kohn, et al., Mitochondria-targeted hydroxyapatite nanoparticles for selective growth inhibition of lung cancer in vitro and in vivo, ACS Appl. Mater. Interfaces. 8 (2016) 25680–25690. doi:10.1021/acsami.6b06094.

[6] F. Ridi, I. Meazzini, B. Castroflorio, M. Bonini, D. Berti, P. Baglioni, Functional calcium phosphate composites in nanomedicine, Adv. Colloid Interface Sci. 244 (2017) 281–295. doi:10.1016/j.cis.2016.03.006.

[7] N.L. Ignjatović, P. Ninkov, R. Sabetrasekh, D.P. Uskoković, A novel nano drug delivery system based on tigecycline-loaded calciumphosphate coated with poly-DL-lactide-co-glycolide, J. Mater. Sci. Mater. Med. 21 (2010) 231–239. doi:10.1007/s10856-009-3854-6.

[8] N. Ignjatović, V. Uskoković, Z. Ajduković, D. Uskoković, Multifunctional hydroxyapatite and poly(d,l-lactide-co-glycolide) nanoparticles for the local delivery of cholecalciferol, Mater. Sci. Eng. C. 33 (2013) 943–950. doi:10.1016/j.msec.2012.11.026.

[9] Z. Li, S. Tan, S. Li, Q. Shen, K. Wang, Cancer drug delivery in the nano era: An overview and perspectives (Review), Oncol. Rep. 38 (2017) 611–624. doi:10.3892/or.2017.5718.

[10] E. Bender, Epidemiology: The dominant malignancy, Nature. 513 (2014) S2–S3. doi:10.1038/513S2a.

[11] S. Wilhelm, A.J. Tavares, Q. Dai, S. Ohta, J. Audet, H.F. Dvorak, et al., Analysis of nanoparticle delivery to tumours, Nat. Rev. Mater. 1 (2016) 16014. doi:10.1038/natrevmats.2016.14.

[12] S. Deshayes, R. Gref, Synthetic and bioinspired cage nanoparticles for drug delivery., Nanomedicine (Lond). 9 (2014) 1545–1564. doi:10.2217/nnm.14.67.

[13] F. Ye, Å. Barrefelt, H. Asem, M. Abedi-Valugerdi, I. El-Serafi, M. Saghafian, et al., Biodegradable polymeric vesicles containing magnetic nanoparticles, quantum dots and anticancer drugs for drug delivery and imaging, Biomaterials. 35 (2014) 3885–3894. doi:10.1016/j.biomaterials.2014.01.041.

[14] N. Arya, D.S. Katti, Poly(d,l-lactide-co-glycolide)-chitosan composite particles for the treatment of lung cancer, Int. J. Nanomedicine. 10 (2015) 2997–3011. doi:10.2147/IJN.S78120.

[15] H.N. Ho, T.H. Tran, T.B. Tran, C.S. Yong, C.N. Nguyen, Optimization and characterization of artesunate-loaded chitosan-decorated poly(D,L-lactide-co-glycolide) acid nanoparticles, J. Nanomater. 2015 (2015). doi:10.1155/2015/674175.

[16] C.K. Thakur, N. Thotakura, R. Kumar, P. Kumar, B. Singh, D. Chitkara, et al., Chitosan-modified PLGA polymeric nanocarriers with better delivery potential for tamoxifen, Int. J. Biol. Macromol. 93 (2016) 381–389. doi:10.1016/j.ijbiomac.2016.08.080.

[17] J.U. Menon, A. Kuriakose, R. Iyer, E. Hernandez, L. Gandee, S. Zhang, et al., Dual-drug containing core-shell nanoparticles for lung cancer therapy, Sci. Rep. 7 (2017) 13249. doi:10.1038/s41598-017-13320-4.

[18] N. Ignjatović, S. Vranješ Djurić, Ž. Mitić, D. Janković, D. Uskoković, Investigating an organ-targeting platform based on hydroxyapatite nanoparticles using a novel in situ method of radioactive 125Iodine labeling, Mater. Sci. Eng. C. 43 (2014) 439–446. doi:10.1016/j.msec.2014.07.046.

[19] S. Vranješ Đurić, N.L. Ignjatović, Radiolabeled functional nanoparticles in preventve and regenerative medicine, in: V. Uskoković, D. Uskoković (Eds.), Nanotechnologies

Prev. Regen. Med., 1st ed., Elsevier, 2018: pp. 1–92. https://doi.org/10.1016/B978-0-323-48063-5.00001-0.

[20] J.J. Ajduković, K.M. Penov Gaši, D.S. Jakimov, O.R. Klisurić, S.S. Jovanović-Šanta, M.N. Sakač, et al., Synthesis, structural analysis and antitumor activity of novel 17α-picolyl and 17(E)-picolinylidene A-modified androstane derivatives, Bioorganic Med. Chem. 23 (2015) 1557–1568. doi:10.1016/j.bmc.2015.02.001.

[21] I. Kuzminac, O.R. Klisurić, D. Škorić, D. Jakimov, M. Sakač, Structural analysis and antitumor potential of novel 5,6-disubstituted-17a-homo-17-oxa-androstane derivatives, Struct. Chem. 28 (2017) 567–576. doi:10.1007/s11224-016-0815-9.

[22] S. Bjedov, D. Jakimov, A. Pilipović, M. Poša, M. Sakač, Antitumor activity of newly synthesized oxo and ethylidene derivatives of bile acids and their amides and oxazolines, Steroids. 120 (2017) 19–25. doi:10.1016/j.steroids.2017.01.008.

[23] N.L. Ignjatović, K.M. Penov-Gaši, V.M. Wu, J.J. Ajduković, V. V. Kojić, D. Vasiljević-Radović, et al., Selective anticancer activity of hydroxyapatite/chitosan-poly(D,L)-lactide-co-glycolide particles loaded with an androstane-based cancer inhibitor, Colloids Surfaces B Biointerfaces. 148 (2016) 629–639. doi:10.1016/j.colsurfb.2016.09.041.

[24] K.M. Penov Gaši, S.M. Stanković, J.J. Csanádi, E.A. Djurendić, M.N. Sakač, L. Medić Mijačević, et al., New D-modified androstane derivatives as aromatase inhibitors, Steroids. 66 (2001) 645–653. doi:10.1016/S0039-128X(01)00096-4.

[25] K.M.P. Gaši, M.D.D. Brenesel, E.A. Djurendić, M.N. Sakač, J.J. Čanadi, J.J. Daljev, et al., Synthesis and biological evaluation of some 17-picolyl and 17-picolinylidene androst-5-ene derivatives, Steroids. 72 (2007) 31–40. doi:10.1016/j.steroids.2006.10.002.

[26] N.L. Ignjatović, C.Z. Liu, J.T. Czernuszka, D.P. Uskoković, Micro- and nano-

injectable composite biomaterials containing calcium phosphate coated with poly(dl-lactide-co-glycolide), Acta Biomater. 3 (2007) 927–935. doi:10.1016/j.actbio.2007.04.001.

[27] T. Mosmann, Rapid colorimetric assay for cellular growth and survival: Application to proliferation and cytotoxicity assays, J. Immunol. Methods. 65 (1983) 55–63. doi:10.1016/0022-1759(83)90303-4.

[28] N. Ignjatović, V. Wu, Z. Ajduković, T. Mihajilov-Krstev, V. Uskoković, D. Uskoković, Chitosan-PLGA polymer blends as coatings for hydroxyapatite nanoparticles and their effect on antimicrobial properties, osteoconductivity and regeneration of osseous tissues, Mater. Sci. Eng. C. 60 (2016) 357–364. doi:10.1016/j.msec.2015.11.061.

[29] G.B. Djigoué, B.T. Ngatcha, J. Roy, D. Poirier, Synthesis of 5α-Androstane-17-spiro-δ-lactones with a 3-keto, 3-hydroxy, 3-spirocarbamate or 3-spiromorpholinone as inhibitors of 17β-hydroxysteroid dehydrogenases, Molecules. 18 (2013) 914–933. doi:10.3390/molecules18010914.

[30] A. Lak, M. Mazloumi, M.S. Mohajerani, S. Zanganeh, M.R. Shayegh, A. Kajbafvala, et al., Rapid formation of mono-dispersed hydroxyapatite nanorods with narrow-size distribution via microwave irradiation, J. Am. Ceram. Soc. 91 (2008) 3580–3584. doi:10.1111/j.1551-2916.2008.02690.x.

[31] S.N. Tammam, H.M.E. Azzazy, H.G. Breitinger, A. Lamprecht, Chitosan nanoparticles for nuclear targeting: the effect of nanoparticle size and nuclear localization sequence density, Mol. Pharm. 12 (2015) 4277–4289. doi:10.1021/acs.molpharmaceut.5b00478.

[32] Y. Shi, J. xue, L. Jia, Q. Du, J. Niu, D. Zhang, Surface-modified PLGA nanoparticles with chitosan for oral delivery of tolbutamide, Colloids Surfaces B Biointerfaces. 161 (2018) 67–72. doi:10.1016/j.colsurfb.2017.10.037.

[33] C.K. Thakur, N. Thotakura, R. Kumar, P. Kumar, B. Singh, D. Chitkara, et al., Chitosan-modified PLGA polymeric nanocarriers with better delivery potential for tamoxifen, Int. J. Biol. Macromol. 93 (2016) 381–389. doi:10.1016/j.ijbiomac.2016.08.080

[34] L.C. Alskär, C.J.H. Porter, C.A.S. Bergström, Tools for early prediction of drug loading in lipid-based formulations, Mol. Pharm. 13 (2016) 251–261. doi:10.1021/acs.molpharmaceut.5b00704.

[35] X. Qu, A. Wirsén, A.C. Albertsson, Effect of lactic/glycolic acid side chains on the thermal degradation kinetics of chitosan derivatives, Polymer (Guildf). 41 (2000) 4841–4847. doi:10.1016/S0032-3861(99)00704-1.

[36] A.T.C.R. Silva, B.C.O. Cardoso, M.E.S.R. e Silva, R.F.S. Freitas, R.G. Sousa, Synthesis, characterization, and study of PLGA copolymer *in vitro* degradation, J. Biomater. Nanobiotechnol. 6 (2015) 8–19. doi:10.4236/jbnb.2015.61002.

[37] A.E. Nel, L. Mädler, D. Velegol, T. Xia, E.M. V. Hoek, P. Somasundaran, et al., Understanding biophysicochemical interactions at the nano–bio interface, Nat. Mater. 8 (2009) 543–557. doi:10.1038/nmat2442.

[38] M. Motskin, D.M. Wright, K. Muller, N. Kyle, T.G. Gard, A.E. Porter, et al., Hydroxyapatite nano and microparticles: Correlation of particle properties with cytotoxicity and biostability, Biomaterials. 30 (2009) 3307–3317. doi:10.1016/j.biomaterials.2009.02.044.

[39] L. Chen, J.M. Mccrate, J.C.-M. Lee, H. Li, The role of surface charge on the uptake and biocompatibility of hydroxyapatite nanoparticles with osteoblast cells, Nanotechnology. 22 (2011) 105708. doi:10.1088/0957-4484/22/10/105708.

[40] S. Yamane, A. Sugawara, Y. Sasaki, K. Akiyoshi, Nanogel-calcium phosphate hybrid nanoparticles with negative or positive charges for potential biomedical applications,

Bull. Chem. Soc. Jpn. 82 (2009) 416–418. doi:10.1246/bcsj.82.416.

[41] R. Xu, Progress in nanoparticles characterization: Sizing and zeta potential measurement, Particuology. 6 (2008) 112–115. doi:10.1016/j.partic.2007.12.002.

[42] V. Uskoković, Dynamic light scattering based microelectrophoresis: main prospects and limitations, J. Dispers. Sci. Technol. 33 (2012) 1762–1786. doi:10.1080/01932691.2011.625523.

[43] Y. Zhang, M. Yang, N.G. Portney, D. Cui, G. Budak, E. Ozbay, et al., Zeta potential: A surface electrical characteristic to probe the interaction of nanoparticles with normal and cancer human breast epithelial cells, Biomed. Microdevices. 10 (2008) 321–328. doi:10.1007/s10544-007-9139-2.

[44] C. Pfeiffer, C. Rehbock, D. Huhn, C. Carrillo-Carrion, D.J. de Aberasturi, V. Merk, et al., Interaction of colloidal nanoparticles with their local environment: the (ionic) nanoenvironment around nanoparticles is different from bulk and determines the physico-chemical properties of the nanoparticles, J. R. Soc. Interface. 11 (2014) 20130931. doi:10.1098/rsif.2013.0931.

[45] R. Bansal, P.C. Acharya, Man-made cytotoxic steroids: Exemplary agents for cancer therapy, Chem. Rev. 114 (2014) 6986–7005. doi:10.1021/cr4002935.

[46] I.O. Farah, Differential modulation of intracellular energetics in A549 and MRC-5 cells, Biomed. Sci. Instrum. 43 (2007) 110-115. PMID: 17487066.

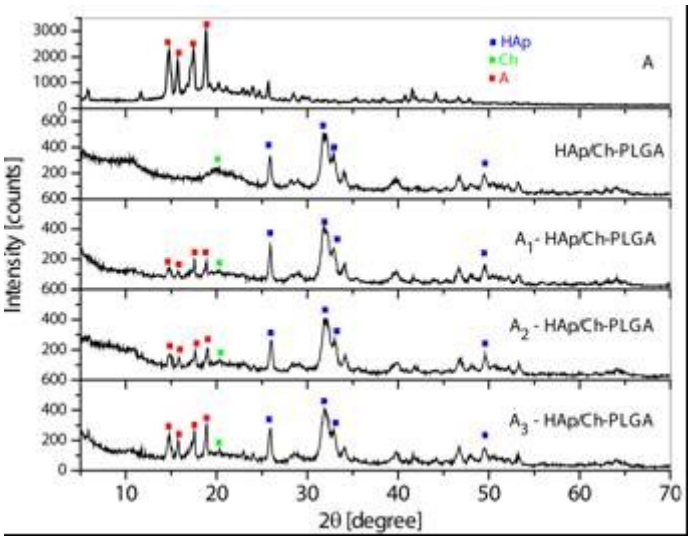

Figure 1

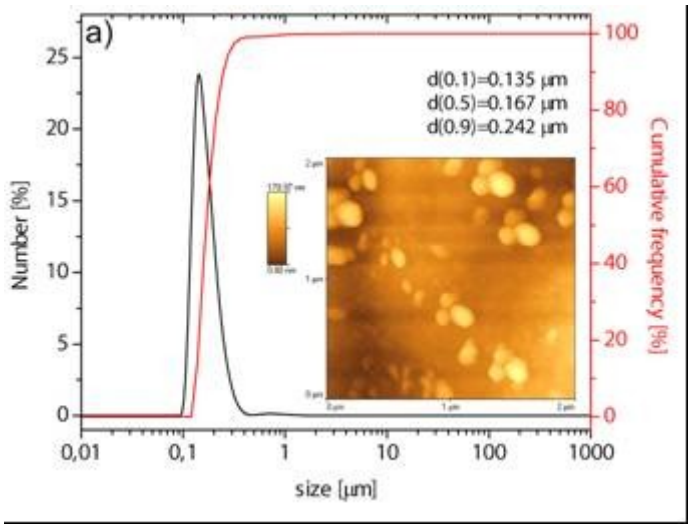

Figure 2a

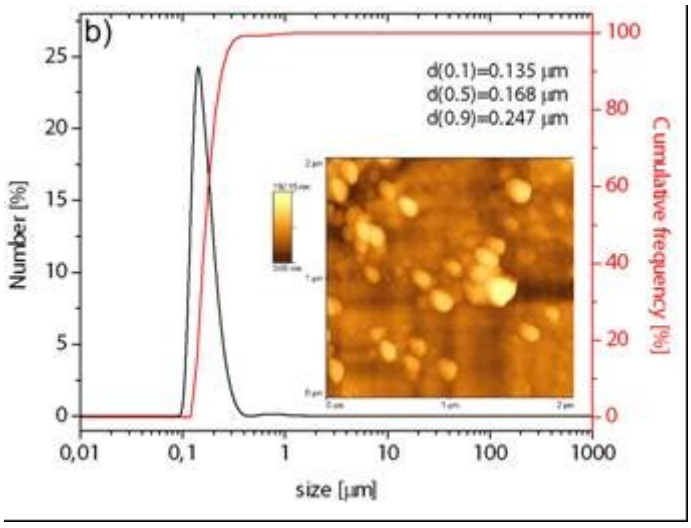

Figure 2b

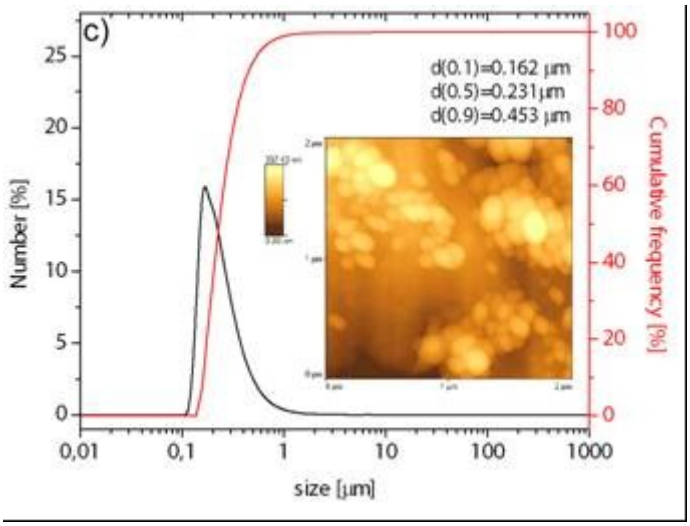

Figure 2c

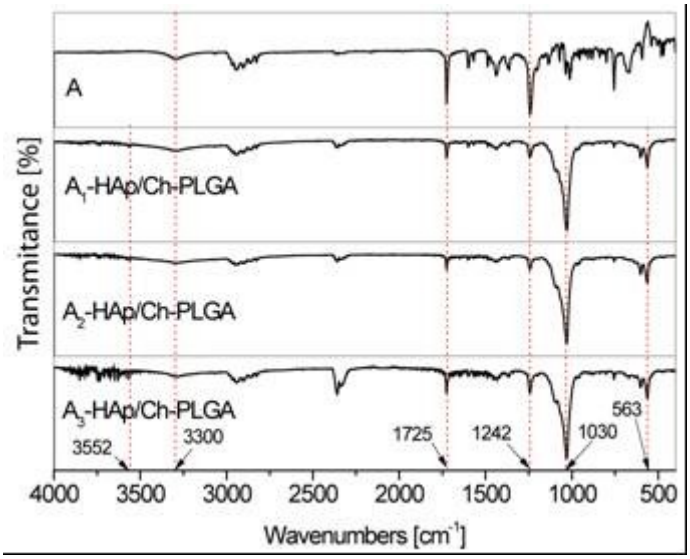

Figure 3

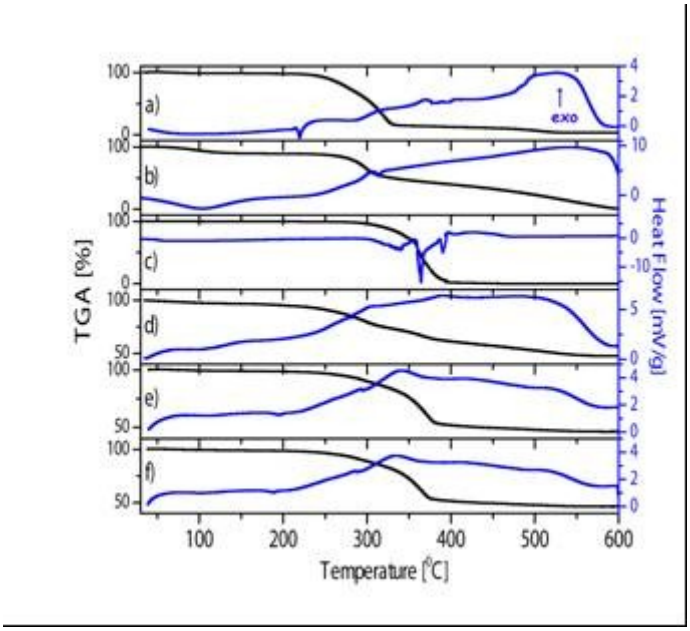

Figure 4

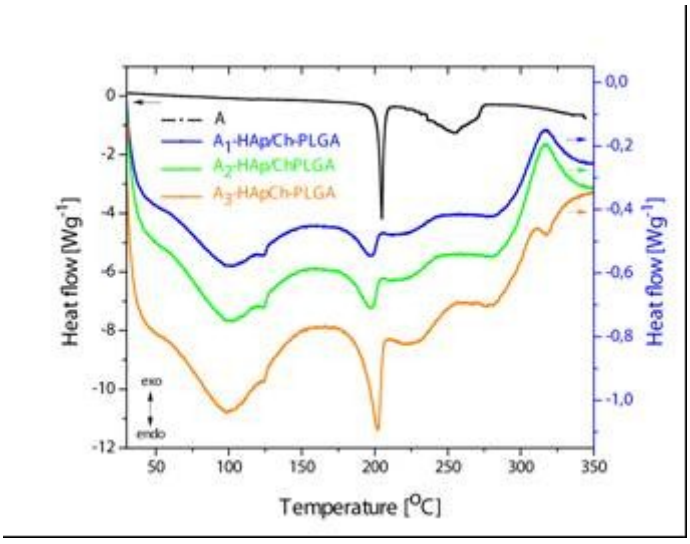

Figure 5

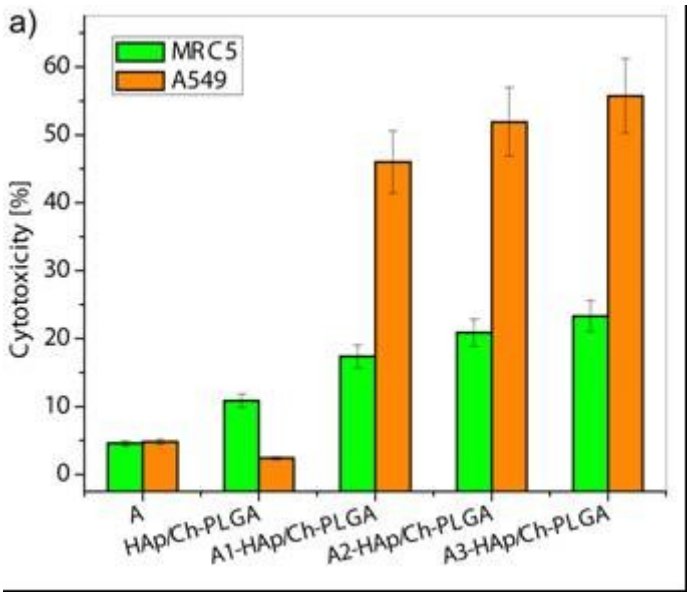

Figure 6a

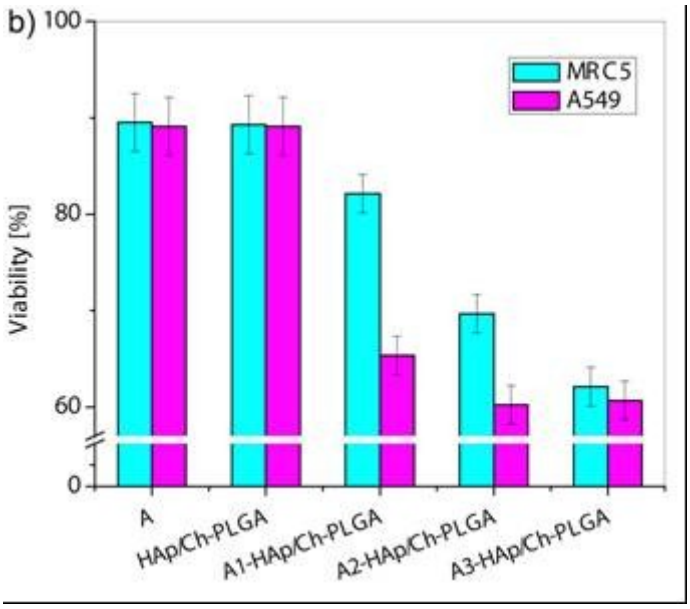

Figure 6b

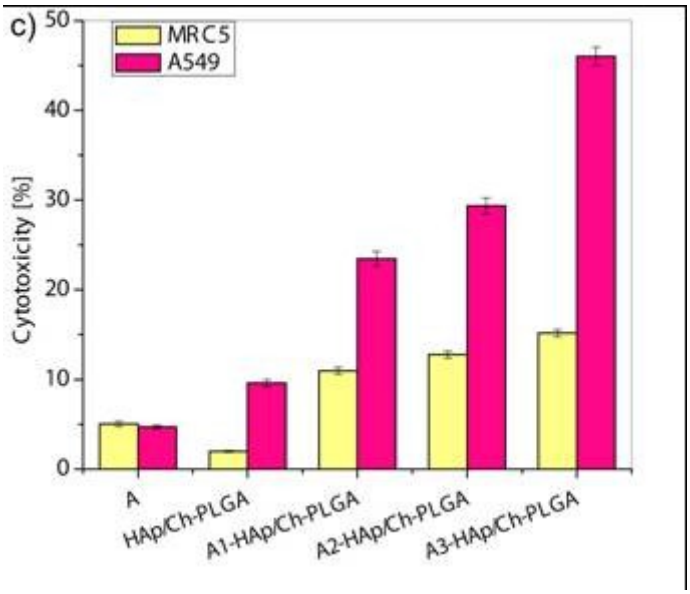

Figure 6c

Table 1

A content [wt %]	Name
10	A_1-HAp/Ch-PLGA
15	A_2-HAp/Ch-PLGA
25	A_3-HAp/Ch-PLGA

Table 2

Name	Enthalpy, ΔH of encapsulated A [J/g]	The content of the encapsulated A [%]
A, pure	81.4	100
A_1-HAp/Ch-PLGA	5.3	6.5
A_2-HAp/Ch-PLGA	7.5	9.2
A_3-HAp/Ch-PLGA	15.7	19.3

Table 3

Name	Temperature [°C]	ξ [mV]	u_e [μmcm/Vs]	K [10^{-3} mS/cm]
A_1-HAp/Ch-PLGA	25	-9.6±0.4	-0.75±0.03	13.9±0.73
A_2-HAp/Ch-PLGA	25	-19.2±1.0	-1.51±0.08	21.5±1.9
A_3-HAp/Ch-PLGA	25	-33.3±2.4	-2.61±0.18	27.2±3.2